A methodology for simulating plasticity induced crack closure and crack shape evolution based on elastic-plastic fracture parameters

Mikel Escalero[a,b,*], Miguel Muniz-Calvente[b], Haritz Zabala[a], Iker Urresti[a], Ricardo Branco[c], FV Antunes[c]

[a] *Ikerlan Technology Research Center, Basque Research and Technology Alliance (BRTA). Pº J.M. Arizmendiarreta, 2, 20500 Arrasate-Mondragón, Spain.*
[b] *Department of Construction and Manufacturing Engineering, University of Oviedo. C\Pedro Puig Adam, s/n, 33204 Gijón, Spain.*
[c] *Univ Coimbra, Centre for Mechanical Engineering, Materials and Processes (CEMMPRE), Department of Mechanical Engineering.*

Abstract

A methodology for simulating plasticity induced crack closure and crack shape evolution based on elastic-plastic fracture parameters is proposed, which represents a new way to predict fatigue crack growth in small and large scale yielding scenarios. The methodology consists in solving iteratively a single elastic-plastic finite element model, for which the load history is kept by remeshing and mapping and crack advance is performed by node releasing. Aiming to illustrate and validate the approach, the growth of an initially straight crack is simulated in a compact tension specimen subjected to small scale yielding conditions, using the plastic crack tip opening displacement range ($\Delta \mathrm{CTOD_p}$) as the crack driving force. The predicted crack shape shows high agreement with experimental observations and the crack opening load trends are consistent with the literature, demonstrating that the methodology proposed can be relevant for further crack growth studies.

Key words: Crack closure, crack shape evolution, elastic-plastic, crack tip opening displacements

*Corresponding author
Email address: mescalero@ikerlan.es (Mikel Escalero)

Nomenclature

Latin characters

a	Crack length (mm)
B	Thickness (mm)
$\mathrm{d}a/\mathrm{d}N$	Crack growth rate (mm/cycle)
E	Young's modulus (GPa)
K	Stress intensity factor ($\mathrm{MPa\,mm^{1/2}}$)
l	Crack tip element size (mm)
P	Load (N)
R	Stress ratio (-)
r_{pD}	Size of the plastic zone (Dugdale's approximation)
S	Stress (-)
W	Width (mm)

Greek characters

β	Proportionality constant between $\Delta\mathrm{CTOD_p}$ and $\mathrm{d}a/\mathrm{d}N$ (-)
ε	Strain (-)
σ	Stress (MPa)
η_{D}	Normalized crack tip element size (Dugdale's approximation)

Subscripts

$()_{\mathrm{eff}}$	Effective
$()_{\mathrm{max}}$	Maximum
$()_{\mathrm{mid}}$	Midplane
$()_{\mathrm{op}}$	Opening
$()_{\mathrm{mid}}$	Midplane
$()_{\mathrm{p}}$	Plastic
$()_{\mathrm{sur}}$	Surface
$()_{\mathrm{y}}$	Yield

Abbreviations

COD	Crack Opening Displacement
CSE	Crack Shape Evolution
CTOD	Crack Tip Opening Displacement
CT	Compact Tension
PICC	Plasticity Induced Crack Closure

1. Introduction and motivation

Critical components of machinery and constructions are commonly subjected to oscillating loads that can lead to fatigue failure. In order to prevent the catastrophic failure of such components it is crucial to understand the evolution of fatigue damage by fracture mechanics approaches in combination with advanced finite element models. Nowadays, one of the main challenges related to this topic is the prediction of fatigue crack growth in components made of ductile metallic materials [1–4], which can deform beyond the elastic limit. Due to the high stresses around the crack tip, strips of permanently deformed material appear along the opposite crack faces during the crack propagation [5]. These plastic strips contact each other through part of the loading cycle, producing a wedging effect known as Plasticity Induced Crack Closure (PICC) [5].

PICC is an intrinsic aspect of the mechanics of growing cracks [6], which explains different phenomena related to the fatigue crack growth rate, such as the influence of stress ratio [7–10], mean stress [11–13] and specimen thickness [9, 14–16]. Furthermore, PICC influences the crack shape evolution (CSE), producing a greater growth retardation (wedging effect) near the free surfaces [17]. There are several studies in the literature devoted to analyze these effects by means of the finite element method, but most of them analyzed both effects, PICC and CSE, independently.

On the one hand, some authors have studied PICC for fixed crack shapes, either straight [18–21] or curved [22, 23]. They considered elastic-plastic material models and followed the strategy originally proposed by Newman (2D) [11] and Chermahini (3D) [24], which consists in the successive release of nodes after applying certain load cycles. This strategy allows to develop the plastic wake as the crack propagates [18] and to determine the crack opening load or stress ($P_{\mathrm{op}}/P_{\mathrm{max}}, S_{\mathrm{op}}/S_{\mathrm{max}}$) that can be used for estimating the value of a crack driving force, such as the effective stress intensity factor range ($\Delta K_{\mathrm{eff}} = K_{\mathrm{max}}\,(1 - P_{\mathrm{op}}/P_{\mathrm{max}})$) [21].

On the other hand, some authors have performed the simulation of CSE by neglecting the influence of PICC [25–27]. The most popular strategy is the multiple point scheme introduced by Smith and Cooper [28] and improved by Lin and Smith [29–31]. According to this strategy, the stress intensity factors are calculated assuming linear elastic material behavior and the new locations of the crack front are obtained based on a fatigue crack growth law, such as that proposed by Paris [32]. Thereafter, the finite element model is remeshed considering the next crack front and a new linear elastic finite element simulation is performed disregarding the plastic wake.

Although the vast majority of published papers have addressed both effects separately, a strong interaction exists between PICC and CSE, as demonstrated by Branco et al. [33]. On one side, Yu and Guo [34] obtained the new crack front by using Elber's equation [35], for which the stress intensity factors were computed numerically with a linear elastic model and the crack opening loads were estimated analytically through the equivalent thickness conception [36]. This approach is efficient because the huge computational effort associated to solving the elastic-plastic model is avoided, but the expressions for determining the crack opening load are usually developed by considering certain hypotheses regarding material, loading and geometry that are not met by generic crack cases [37]. On the other side, various authors have proposed methodologies for the simultaneous simulation of PICC and CSE [17, 38–40] by following basically the same strategy. For each crack front, two geometrically identical models are solved: one with the linear elastic material properties to determine the maximum

stress intensity factors along the crack front and another one with the elastic-plastic behavior of the material to obtain the crack opening loads. After that, the results of both models are combined through an effective stress intensity factor range and the Elber's crack growth law in order to determine the crack growth increments along the crack front and, therefore, the fatigue crack shape evolution.

A considerable part of the research related to the simultaneous simulation of PICC and CSE has focused on the development of numerical techniques for keeping the load history information in the elastic-plastic model while changing the crack shape. Hou suggested the free-front technique [38], Gardin employed node release [17] and remeshing [40] strategies and Gozin [39] and Hou [41] proposed the remeshing and mapping technique. Nevertheless, all these authors determined the new crack front based on the effective stress intensity factor range, which implies two relevant shortcomings: 1) the numerical effort devoted to solve two different finite element models (elastic and elastic-plastic) and 2) the limited applicability to small scale yielding scenarios. Both limitations can be overcome by using elastic-plastic fracture parameters for simulating fatigue crack growth, which would permit to perform predictions with a single finite element model and address large scale yielding situations inherent to high loads [42, 43], low-resistance materials [13] and short cracks [44–46].

The objective of this study is to develop and validate a methodology for the simulation of plasticity induced crack closure and crack shape evolution based on elastic-plastic fracture parameters. In this paper, the plastic crack tip opening displacement range ($\Delta \mathrm{CTOD_p}$) is selected as the crack driving force, because its relationship with the fatigue crack growth rate is linear [47, 48] and, therefore, the fatigue CSE and PICC can be predicted along the crack front without experimental characterization of the fatigue crack growth rate.

2. Proposed methodology

The proposed methodology allows to simulate PICC and CSE simultaneously by solving iteratively a single elastic-plastic finite element model that keeps the load history information by remeshing and mapping techniques [39, 41] and performs the crack advance by node releasing. The main steps of the methodology are shown in the flowchart presented in Figure 1 and explained below.

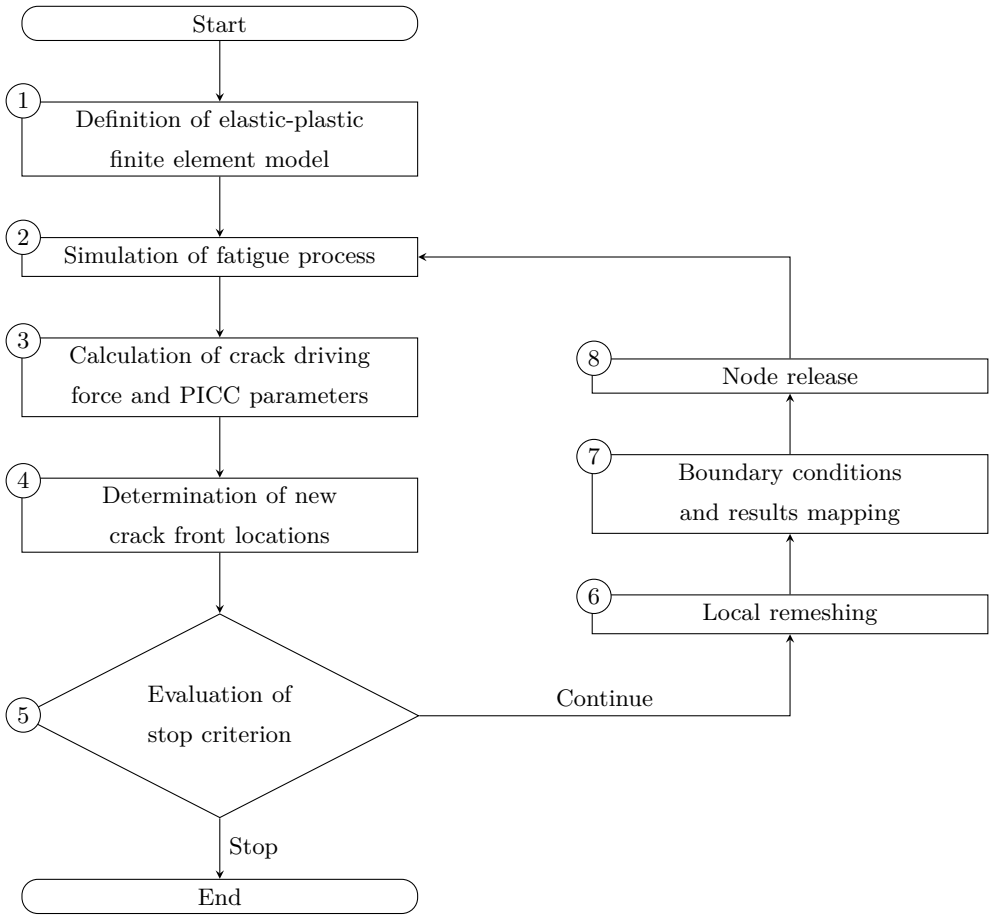

Figure 1: Flowchart of the proposed methodology.

2.1. Definition of elastic-plastic finite element model

First of all, the linear elastic properties and the hysteretic behavior of the material have to be defined. In this study the Von Mises yield criterion was used combined with the Chaboche hardening law (Equation 1), which is appropriate for representing metals that display kinematic hardening [49].

$$\mathrm{d}\mathbf{X} = C_x \left[X_{\mathrm{sat}} \frac{\boldsymbol{\sigma}' - \mathbf{X}}{\bar{\sigma}} - \mathbf{X} \right] \mathrm{d}\bar{\varepsilon}^{\mathrm{p}} \tag{1}$$

$\mathbf{X}$ is the backstress tensor and $\boldsymbol{\sigma}'$ is the deviatoric component of the Cauchy stress tensor. $\bar{\varepsilon}^{\mathrm{p}}$ and $\bar{\sigma}$ are the equivalent plastic strain and the equivalent stress, respectively, while C_x and X_{sat} are fitting parameters that can be determined by the optimization algorithm explained in [49].

Regarding the discretization of the geometry, a finite element mesh consisting of global and local regions is advisable (Figure 2a). The local region is formed by a structured mesh composed by linear hexahedral elements along the crack front, as it is common for the three-dimensional crack closure analysis [19, 21, 38]. The elements are completely regular at the crack front region where the material is expected to yield (Figure 2b), and that regular region is big enough to engulf the biggest plastic zone calculated throughout the propagation. Out of the regular region, the size of the elements is increased

gradually towards the boundaries with the global mesh (Figure 2b).

The local mesh may also have a size bias in the thickness direction (Figure 2b). This is appropriate, for example, when the face of the model represents the surface of the body, because the displacement field and the derived results change more abruptly towards the edge [40]. The proposed approach does not require to compute stress intensity factors at the crack front nodes, so more elaborated meshes with singular crack tip elements [38] or spider-web [33] patterns are avoided.

A bonded contact ties the local and global meshes through the interface (Figure 2a). This allows a mesh discontinuity, that is, the adjacent nodes do not have to coincide necessarily, so the topology of the local mesh can be changed without having to alter the global portion. However, this is a numerical artifact that may lead to small irregularities in derived results such as stresses and strains, and therefore should be placed far enough from the crack front.

The plasticity induced crack closure is simulated through the frictionless contact between the fracture-plane solid elements of the local mesh and a rigid surface (not shown in Figure 2) [50].

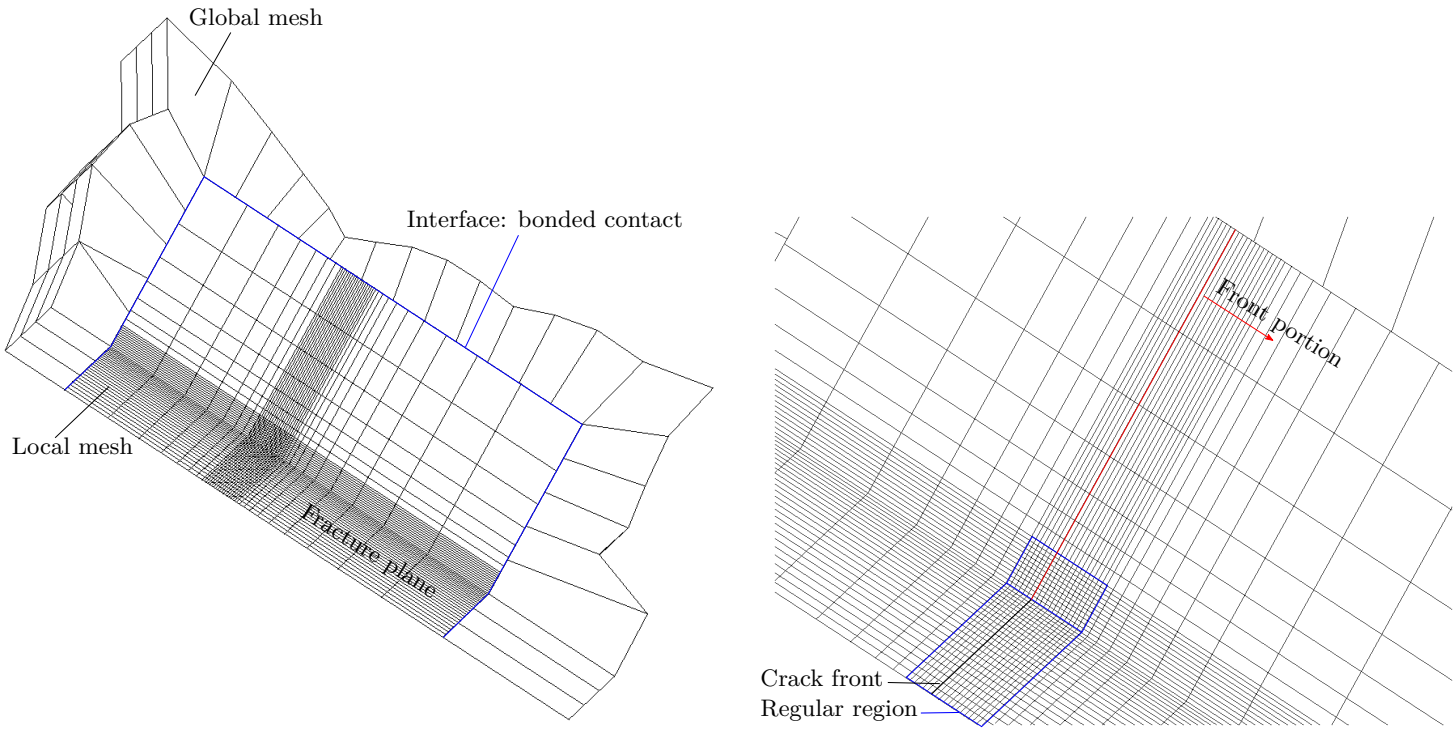

(a) Local and global meshes.

(b) Detail of the local mesh.

Figure 2: Regions of the finite element mesh.

Finally, it is remarkable that various numerical parameters can play an important role on the definition of the elastic-plastic finite element model. The most relevant ones are the type and size of the elements at the regular region of the local mesh and the penetration allowed in the frictionless contact that simulates PICC. Table 1 summarizes the values adopted in recent works that considered PICC in through-cracks.

Table 1: Numerical parameters of the elastic-plastic model for analyzing through-cracks.

			Branco et al. [33]	Camas et al. [50, 51]	Gardin et al. [17, 40]	Hou [52]	Present study
Case of study		Geometry	MT specimen	CT specimen	CT specimen	MT specimen	CT specimen
		Loads: $K_{\max}$	6.97 MPa$\sqrt{\text{mm}}$	25 MPa$\sqrt{\text{mm}}$	13.33 MPa$\sqrt{\text{mm}}$	16.76 MPa$\sqrt{\text{mm}}$	11.94 MPa$\sqrt{\text{mm}}$
		Material: σ_{y}	124 MPa (AA6016-T4)	425 MPa (AA2024-T351)	117 MPa (304L steel)	360 MPa	361.62 MPa (S275 steel)
Numerical parameters	Crack tip elements	Type	Linear hexahedral				
		Integration	Selective reduced	Not defined	Selective reduced	Not defined	Selective reduced
		In-plane size: η_{D}, l	155, 8 µm	90, 15.1 µm [50] 33, 41.2 µm for node contact criterion [51]	102, 50 µm [17] 51, 100 µm [40]	42.55, 20 µm	50, 8.56 µm
		Divisions in half-thickness	5 ($B/2 = 0.5$ mm)	40 30 is concluded to be enough [50] ($B/2 = 1.5$ mm)	20 ($B/2 = 5$ mm)	25 ($B/2 = 1$ mm)	25 ($B/2 = 1.2$ mm)
	Contact	Maximum penetration	Not defined	5e-5 mm	Not defined	Closure is not detected through contact	5e-5 mm
	Loading	Cycles between releases	2	1 (8 after the last release)	15 (30 for the first four releases) [17] 5 [40]	1	1
		No. of substeps	Not defined	40	50 (unevenly distributed) [17]	40	80

2.2. Simulation of fatigue process

In this step, the loading history is simulated by applying the corresponding boundary conditions and cyclic loadings (Figure 3). Typically, several cycles should be simulated in order to stabilize the material response and obtain stationary values of the studied variables ($\Delta\text{CTOD}_{\text{p}}$ and $P_{\text{op}}/P_{\max}$). The optimal number of cycles is still unclear, as it can be concluded from the drastically different values adopted in the literature (Table 1), and is frequently limited by the available computer resources [21].

The high computational cost is caused by the non-linearities of the problem, namely, the elastic-plastic behavior of the material, the frictionless contact and the large displacements. The Newton-Raphson scheme is employed to solve the compatible system of equations resulting from each load step, because it has been the preferred method [50].

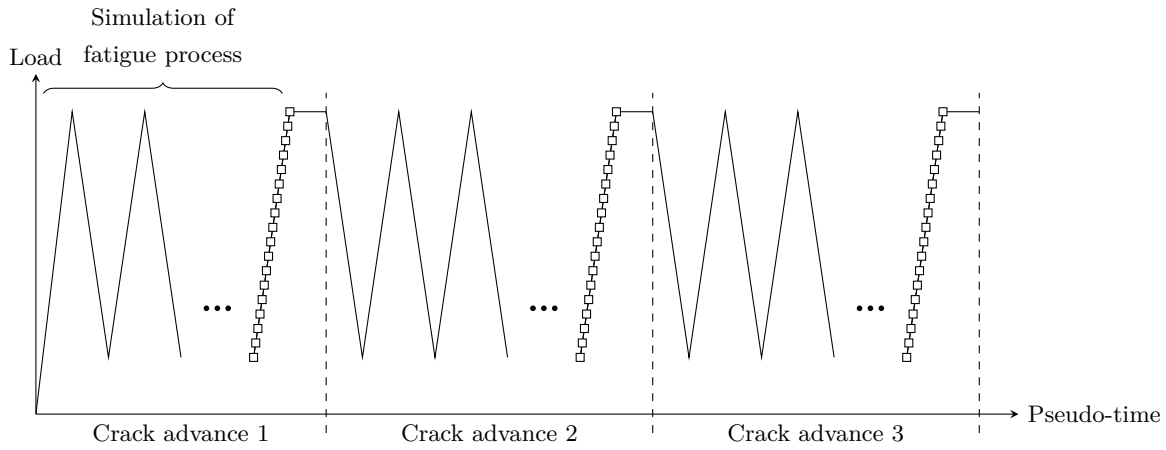

Figure 3: Schematic illustration of the applied load cycles.

2.3. Calculation of crack driving force and PICC parameters

In this study, CTOD is defined as the vertical (perpendicular to the fracture plane) displacement of the nearest node behind each crack-front node [49] (Figure 6), while the mesh dependence introduced by such definition can be avoided by being consistent in the choice of the same crack-tip element size in characterization and prediction crack configurations.

$\Delta\text{CTOD}_\text{p}$ is extracted from the last loading ramp before the node release. For that, 1) the initial elastic region part is identified, 2) a linear fit is performed to obtain the elastic component and 3) the difference between total CTOD and elastic CTOD is obtained at maximum load [47]. This simple procedure contrasts with the energetic methods employed for calculating stress intensity factors, which imply the evaluation of domain integrals over contours of elements around the crack front [53].

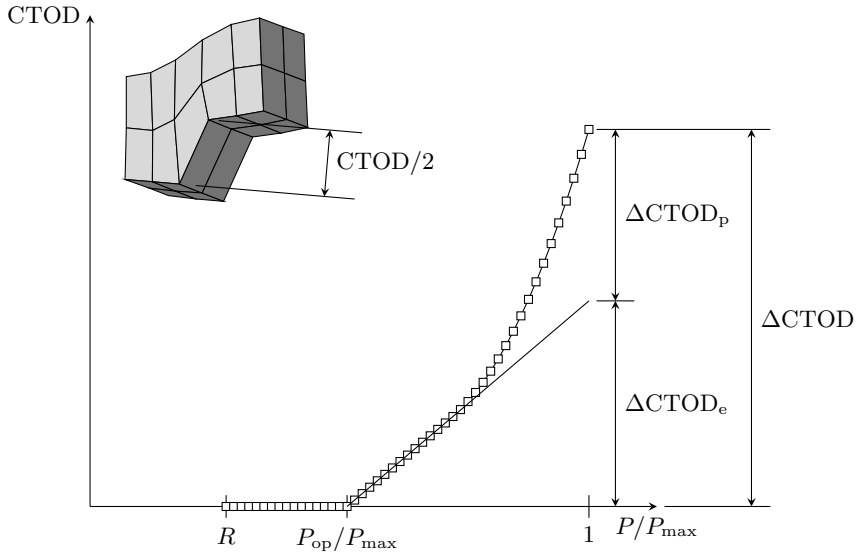

Figure 4: Crack tip opening displacement measured in the first node behind the crack front in the last loading ramp.

Additionally, the crack opening load is calculated even if it is not necessary for the proposed methodology, because it allows a direct comparison and validation against other approaches available for the 3D elastic-plastic simulation of FCG. For that, the moment of detachment of the nearest node from the contact surface is identified, as shown in Figure 4.

2.4. Determination of new crack front locations

The new crack front locations are determined based on the local crack advances and the normal directions. On one side, the crack advances are computed based on the relative advances derived from the linear relationship found by Vasco-Olmo et al. [48], postulating a surface crack increment ($\mathrm{d}a_{\mathrm{sur}}$) of approximately 1.5 times the crack-tip element size. As deduced from Equation 2, such relative crack advances are independent of the proportionality constant β, what supposes an advantage to predict the crack shape evolution without calibrating the crack growth law, unlike other fracture parameters such as ΔK_{eff}.

$$\frac{\mathrm{d}a}{\mathrm{d}N} = \beta \Delta \mathrm{CTOD}_{\mathrm{p}} \rightarrow \frac{\mathrm{d}a_i}{\mathrm{d}a_{\mathrm{sur}}} = \frac{\Delta \mathrm{CTOD}_{\mathrm{p},i}}{\Delta \mathrm{CTOD}_{\mathrm{p,sur}}} \tag{2}$$

On the other side, the normal directions are established by the following unitary vector, where s_i is the local slope determined by the analytical derivation of a cubic splines function fitted to the present crack front locations [4].

$$\vec{n}_i = \begin{bmatrix} \frac{-s_i}{\sqrt{1+s_i^2}} \\ \frac{1}{\sqrt{1+s_i^2}} \end{bmatrix}_{zx} \tag{3}$$

2.5. Evaluation of stop criterion

Before remeshing, mapping and releasing nodes in order to simulate a new crack advance, a stop criterion is evaluated to check if the crack length has reached a critical value, which can be predefined by design requirements or determined by a fracture assessment.

2.6. Local remeshing

In this step, the topology of the front portion of the local mesh is adapted to the shape of the new crack. For that, the existing nodes are moved while keeping the present element connectivity, what means that the overall number of nodes and elements is maintained while the simulated crack propagates.

The remeshing starts by fitting with a cubic splines function the new crack locations, which may display undesired irregularities due to numerical errors or may fall outside the mesh boundaries (Figure 5a). Then, the fitting function is evaluated at the locations of interest, so that the definitive interpolated locations keep the present through-the-thickness bias (Figure 5a).

Once the locations of the new crack front nodes are known, the positions for measuring the crack tip opening displacements for the new crack front are determined, by considering the backward normal directions and a distance equal to the original element size to be consistent in the definition of CTOD (Figure 5b). In order to obtain the location of the surface node a linear extrapolation is performed using the information of the two adjacent locations (Figure 5b).

Finally, the new mesh is created considering the locations calculated for the first two new rows ahead of the present crack (Figure 5c). Beyond the new second row, the rows of nodes are placed by replicating the exact geometry and through-the-thickness distribution of the new crack front. The distance between rows is kept constant for various rows of the new regular region and then it is gradually increased within the new transition region. Note that the nodes at different layers along the y direction are moved to the same xz positions of the nodes at the fracture plane, in order to avoid distorted elements.

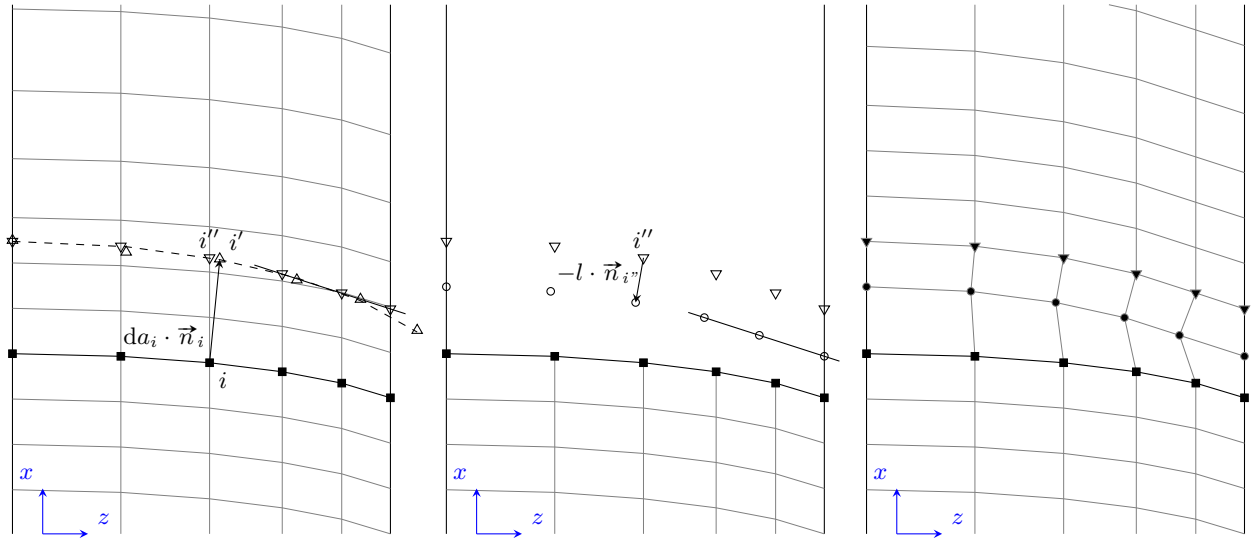

- Present crack front nodes
- Calculated new locations
- Interpolated new locations

(a) New crack front locations.

- Present crack front nodes
- Interpolated new locations
- Locations for measuring CTOD

(b) Locations for measuring CTOD.

- Present crack front nodes
- New crack front nodes
- Nodes for measuring CTOD

(c) New mesh on fracture plane.

Figure 5: Remeshing procedure for the nodes on the fracture plane.

2.7. Boundary conditions and results mapping

The boundary conditions and finite element results are mapped from the old local mesh to the new one in order to transfer the load history information. The nodal displacements for the new nodes are interpolated from the displacements of the old nodes, considering the new node positions and the shape functions of the old elements [41]. The stress and backstress tensor components and the equivalent plastic strain are interpolated for the Gauss integration points of the new elements (see Hou [41]).

The mapping of state variables based on interpolation algorithms does not consider equilibrium conditions. As a consequence, the model has to be solved to balance the residual forces resulting from the mismatch between the internal nodal forces calculated from the interpolated Gauss point stresses and the external nodal forces [54]. The remeshing and mapping operation is performed at

maximum load, when no contact is expected between the nodes of the crack face and the rigid surface, for fostering the numerical convergence in the balancing iterations.

The result of this step is a mesh with nodes in the locations of the new crack front and the CTOD measuring positions, for which the stress-strain state associated to the applied loading history is known.

2.8. Node release

In the last step of each crack advance, the first two rows of nodes are released: 1) the present crack front nodes and 2) the nodes for measuring CTOD for the new crack front. Each row is released separately, by applying at least one cycle between releases in order to avoid a saw-tooth shape of the crack faces. In this way, each release corresponds to an increment of the surface node lower than the the crack-tip element size, what is consistent with the literature [39, 40, 52].

The result of this step is a finite element model with an updated crack front shape, defined by the selected driving force ($\Delta\text{CTOD}_\text{p}$) without losing the load history information. After this step, the model is ready to start a new crack advance coming back to step 2 (Figure 1).

3. Application to a practical example

The methodology is illustrated by the simulation of the fatigue crack growth in a compact tension specimen made of S275 steel and subjected to constant amplitude loading.

3.1. Geometry, loads and material

The fatigue growth of an initially straight 12 mm-long through-crack was predicted in a standard compact tension specimen [55] ($W = 48$ mm, $B = 2.4$ mm).

A cyclic load applied through the pins with a constant amplitude and a ratio of 0.1 was considered. The maximum value was chosen so that the maximum nominal stress intensity factor calculated with analytical approximations [55] would be 12 MPa$\sqrt{\text{m}}$ for the initial crack. These crack length and loading magnitudes reproduced the testing conditions at the beginning of a typical experiment for characterizing fatigue crack growth rates.

The S275 steel, a low-carbon structural steel widely employed in the construction of metallic machinery and structures due to its weldability and malleability [56], was studied. The main material properties needed for the elastic-plastic finite element model are summarized in Table 2.

Table 2: Material properties of the S275 steel.

Young's modulus, E [GPa]	Yield strength, σ_y [MPa]	Chaboche parameters	
		C_x [-]	X_sat [MPa]
200	361.62	133.33	124.24

These values were obtained by fitting the results of low cycle fatigue tests performed on cylindrical dog bone specimens at room temperature [57], under a strain ratio (R_ε) of -1 and three different strain ranges ($\Delta\varepsilon = 3\%, 4\%, 5\%$).

3.2. Finite element model

The finite element model of the CT specimen was generated in ANSYS (Figure 6a). Only one quarter of the cracked body was modeled explicitly, by considering the symmetries at half thickness and the fracture plane. A rigid surface was placed on the fracture plane to simulate PICC through contact (Figure 6a).

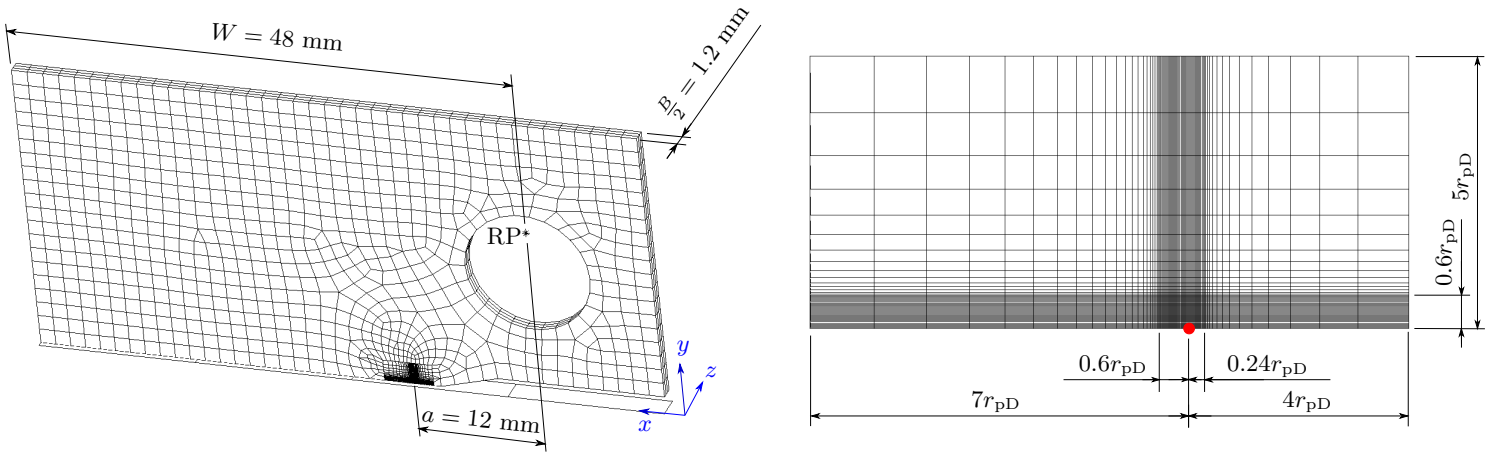

(a) Global mesh dimensions.

(b) Local mesh dimensions.

Figure 6: Initial mesh for the CT specimen.

The mesh for the quarter CT comprised two parts: a fine local mesh in the crack front region and a coarse global mesh that represented the main geometrical features of the specimen. The relevant mesh dimensions were determined based on an approximate plastic zone size estimated with Dugdale's expression for plane stress conditions (Equation 4) [50].

$$r_{\mathrm{pD}} = \frac{\pi}{8}\left(\frac{K_{\max}}{\sigma_{\mathrm{y}}}\right)^2 = 0.428 \text{ mm} \tag{4}$$

The local mesh was $11r_{\mathrm{pD}}$ long and $5r_{\mathrm{pD}}$ high (Figure 6b) and consisted of 113625 elements (121992 nodes). These elements were linear hexahedral and their stiffness matrices were computed using the selective reduced integration scheme, as recommended by the most recent literature (Table 1).

The regular region of the local mesh was $0.6r_{\mathrm{pD}}$ high and was distributed unsymmetrically with respect to the crack front (Figure 6b). All the elements of the regular region (31500 out of 113625) had in-plane dimensions of 8.56 µm × 8.56 µm, what corresponds to a normalized size $\eta_{\mathrm{D}} = r_{\mathrm{pD}}/l$ equal to 50. This can be considered as an intermediate size in view of the different values ranging between 33 and 155 that have been assigned in the literature (Table 1).

The thickness of the local mesh ($B/2 = 1.2$ mm) was divided in 25 layers of elements. This requirement is similar to Camas', who concluded that 30 elements in a half-thickness of 1.5 mm should be enough (Table 1). Hou's discretization was slightly stricter, because he employed 25 elements in a half-thickness of 1 mm, but Gardin et al. used fewer elements (20) for a bigger thickness ($B/2 = 5$ mm).

The global mesh was built using around 2400 quadratic hexahedral elements, which had around 13000 corner and midside nodes. That mesh was generated by sweeping a 2D topology and was divided in three through-the-thickness element layers (Figure 6a).

The rigid surface used for simulating PICC was discretized by four two-dimensional target elements and slave elements were overlaid over the elements of the local mesh that were on the fracture plane. A frictionless behavior was established, allowing a maximum penetration of 5e-5 mm [50].

3.3. Testing and measurement of beachmarks

In order to validate the crack shape predictions made by the proposed methodology, a compact tension specimen was tested in load control under a sinusoidal force (10 Hz), in an MTS Bionix servo-hydraulic testing machine. The nominal crack-length was estimated through the crack opening displacement (COD) measured with an MTS 632.03C-30 extensometer.

The beachmark was marked by heat tinting at a nominal crack advance of 1.5 mm, by introducing the specimen in an oven for 30 minutes at 300°C, as recommended by ASTM E1820 [58]. Finally, the specimen was subjected to cyclic loading until its total fracture and the fracture surface was studied in a Leica M205 C optical microscope.

4. Results

Figure 7 shows the development of the plastic zone around the growing crack, in terms of Von Mises stresses and equivalent plastic strains. At the beginning, the plastic zone existed ahead of the crack front exclusively, but as the crack advanced, a plastic wake generated behind. In fact, this plastic wake was the responsible for the plasticity induced crack closure through the contact with the rigid surface of the fracture plane, which produced the crack shape change.

In this study, 30 crack advances were completed, leading to a total surface crack advance bigger than twice the maximum size of the initial plastic zone, what fulfilled Camas' requirement to propagate the crack at least $1r_{\mathrm{pD}}$ [50] for obtaining stable values of PICC parameters.

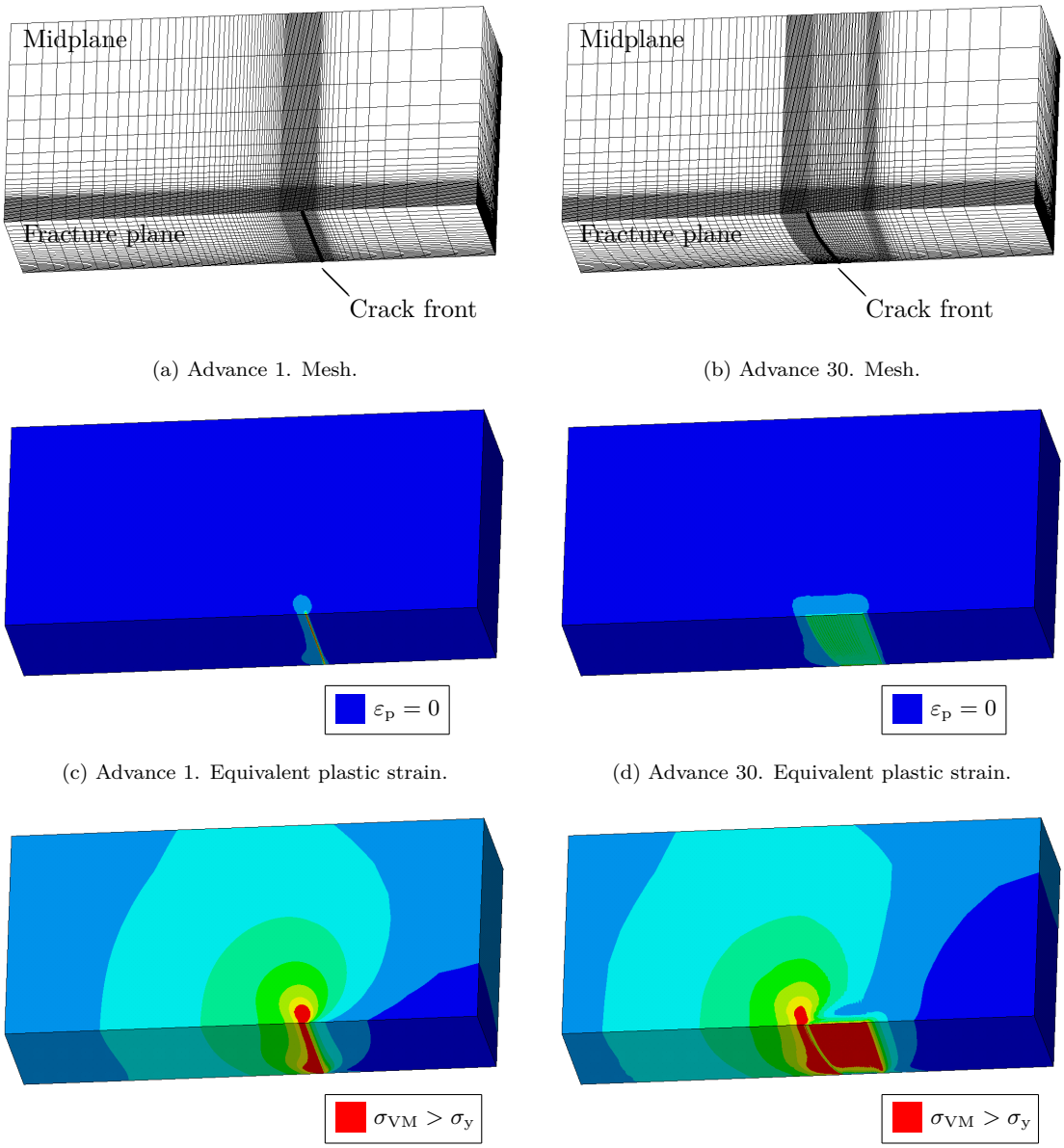

(a) Advance 1. Mesh.

(b) Advance 30. Mesh.

(c) Advance 1. Equivalent plastic strain.

(d) Advance 30. Equivalent plastic strain.

(e) Advance 1. Von Mises stress.

(f) Advance 30. Von Mises stress.

Figure 7: Local mesh, equivalent plastic strain and Von Mises stress for the first and last crack advances.

4.1. Crack shape evolution

4.1.1. Evolution of $\Delta\text{CTOD}_\text{p}$

According to the proposed methodology, each new crack front depends on $\Delta\text{CTOD}_\text{p}$ exclusively, so a detailed analysis of this elastic-plastic fracture parameter is essential to understand the crack shape evolution.

Initially, $\Delta\text{CTOD}_\text{p}$ was relatively constant in great part of the thickness and decreased towards the surface in a 200 µm-wide surface region. Throughout the first six advances (Figure 8a), $\Delta\text{CTOD}_\text{p}$

increased in the bulk region (0 mm $< z <$ 1 mm), whereas the opposite trend was observed in the surface region (1 mm $< z <$ 1.2 mm).

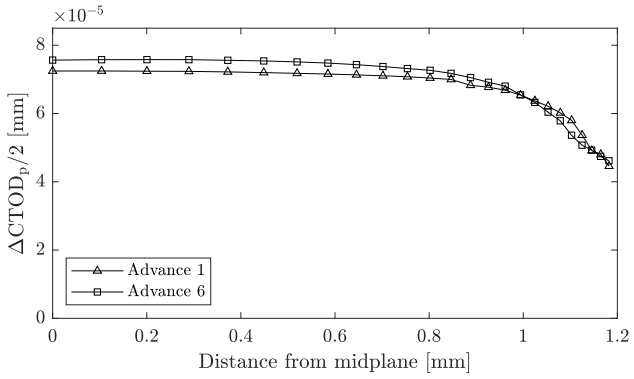

(a) Advances 1 and 6.

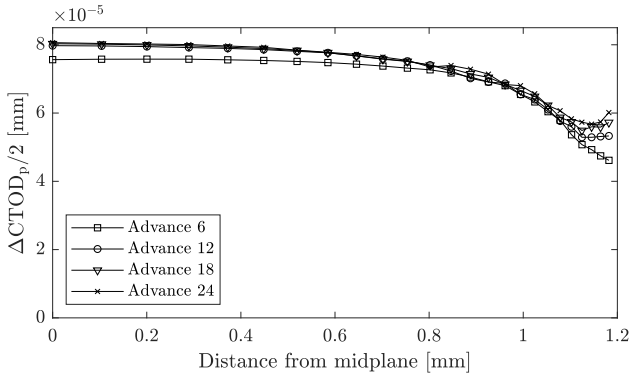

(b) Advances 6, 12, 18 and 24.

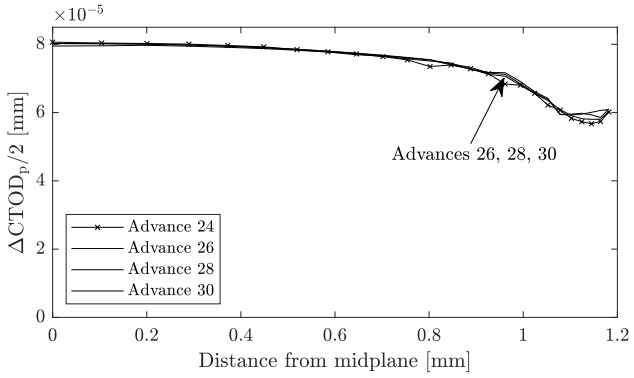

(c) Advances 24, 26, 28 and 30.

Figure 8: Predicted evolution of $\Delta\text{CTOD}_\text{p}$.

From Advance 6 on, $\Delta\text{CTOD}_\text{p}$ increased along the entire crack front, until a stable distribution was achieved. Such stabilization was reached rapidly at Advance 12 in the bulk region (Figure 8b) and later at Advance 24 in the surface region (Figure 8c). From Advance 24 to 30, the stable distribution of $\Delta\text{CTOD}_\text{p}$ displayed a relatively flat bulk region, followed by a decrease at a distance of 1 mm from

the midplane, with a plateau close to the surface (Figure 8c).

4.1.2. Predicted beachmarks and experimental correlation

Figure 9 shows the crack shape evolution predicted based on $\Delta\text{CTOD}_\text{p}$. The total crack advance was approximately 600 µm at the midplane and 410 µm at the surface, reproducing the expected progressive curvature of the crack front.

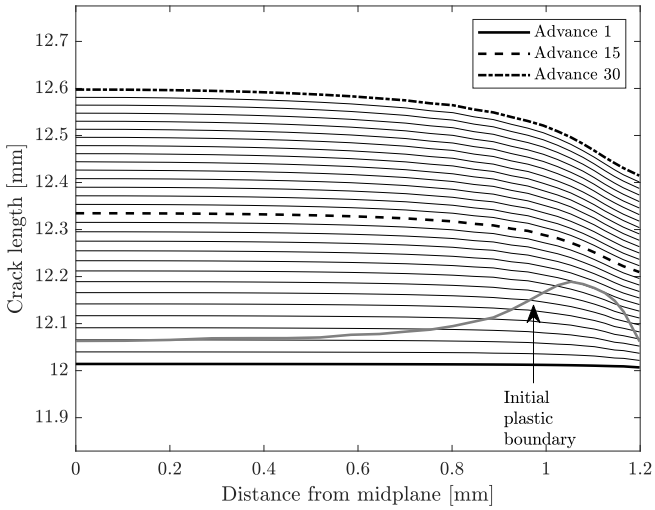

Figure 9: Predicted evolution of beachmarks.

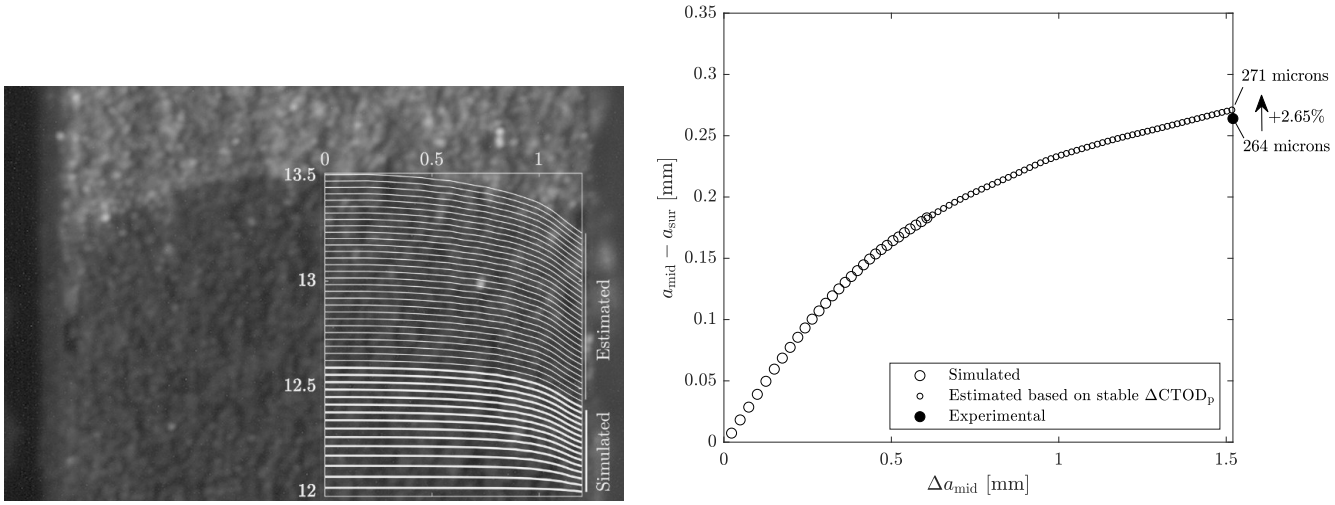

(a) Beachmarks.

(b) Tunneling distance.

Figure 10: Comparison between predicted and experimental beachmarks and tunneling distance.

Given the high computational cost of the simulations, the crack propagation from $\Delta a_{\text{mid}} = 600$ µm

to 1.5 mm was estimated based on the stable $\Delta CTOD_p$ distribution of the last simulated crack advance (Figure 10a). The tunneling distance at the end of the crack propagation was determined with an error of 2.65% (Figure 10b), what supported the validity of the proposed methodology and the suitability of $\Delta CTOD_p$ as the crack driving force.

4.2. Evolution of plasticity induced crack closure

In this section, the evolution of the crack opening load (P_{op}/P_{max}) is studied as the the most representative parameter of the plasticity induced crack closure [50].

As already observed for $\Delta CTOD_p$, the P_{op}/P_{max} distribution displayed well differentiated bulk and surface regions. Initially, from Advances 1 to 8 (Figure 11a), the crack opening load decreased in the bulk region, whereas it increased in the surface region. Then, the trend inverted in the bulk region, so as the crack propagated from Advance 8 onwards, the crack opening load increased throughout the entire crack front (Figure 11b). Finally, at Advance 20 a stable through-the-thickness distribution was reached, which suffered very small variations up to the last crack advance (Figure 11c). The converged values were around 0.21 and 0.56 for the midplane and the surface, what agrees with the literature that reported values around 0.2-0.35 for the midplane and 0.55-0.65 for the surface under the same stress ratio [33, 50, 52].

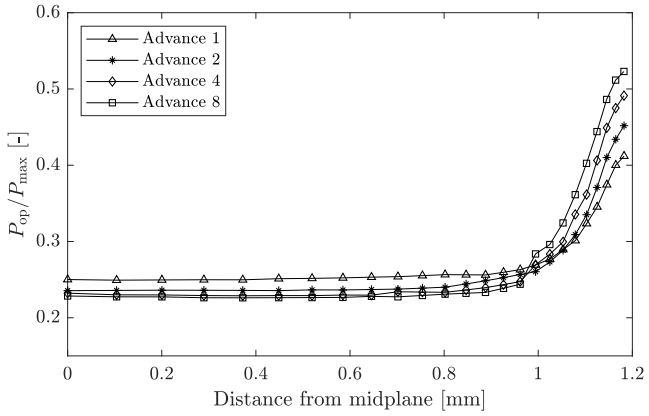

(a) Advances 1, 2, 4 and 8.

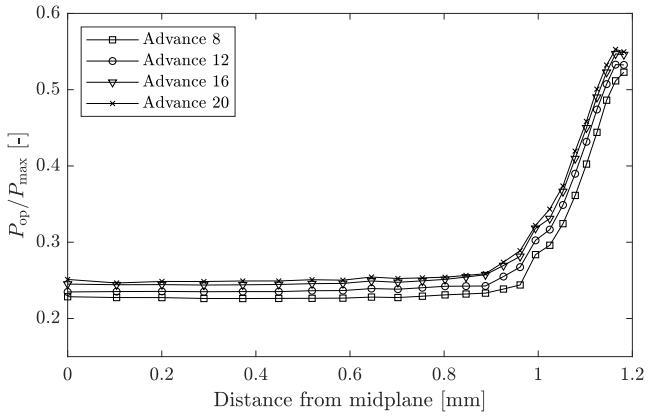

(b) Advances 8, 12, 16 and 20.

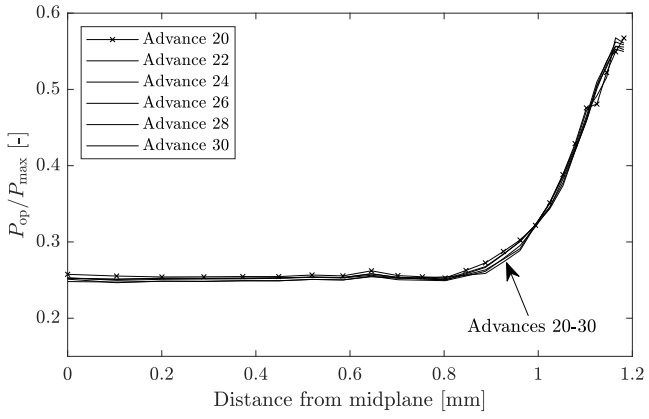

(c) Advances 20, 22, 24, 26, 28 and 30.

Figure 11: Predicted evolution of P_{op}/P_{max}.

5. Discussion

As far as the present authors know, this is the first study that performs a 3D finite element analysis to calculate the distribution of $\Delta\text{CTOD}_\text{p}$ through the thickness. Therefore, it is relevant to compare the results obtained in this paper with the trends observed for other crack driving forces, such as ΔK_eff, which was used by several authors to perform simultaneous simulations of PICC and CSE.

For instance, Gardin et al. simulated the growth of an initially straight through-crack in a compact tension specimen, by considering fixed straight [17] and evolving curved [17, 40] shapes. For the fixed straight crack, ΔK_eff was relatively constant throughout a long region in the half-thickness and then it decreased towards the surface. As the crack advanced, ΔK_eff increased in the bulk region but decreased in the surface region. These are exactly the same trends observed for $\Delta\text{CTOD}_\text{p}$ at the first six crack advances, where the straight crack assumption may still apply. For the evolving crack, Gardin et al. found a faster increment of ΔK_eff at the surface during the initial phase and, after certain propagation, a minimum value was observed close to the surface. They reached a stable through-the-thickness configuration where the differences between the minimum and maximum values were around 18% [40], what permitted to ratify ΔK_eff as the crack driving force. Here the same trends were identified, even if $\Delta\text{CTOD}_\text{p}$ still presented through-the-thickness variations at the last simulated crack advance. More specifically, the minimum value was 27% lower than the midplane value.

Moving to the crack opening load (P_op/P_max), Branco et al. found that the crack closure developed next to the surface resulted in an increase of the crack opening load as the crack grew [33]. Concerning the distribution along the thickness, Camas [50] reported a sudden increment of the crack opening load in the 250 µm-long region close to the surface in a 3 mm-thick specimen. The studied materials and load levels were different, but the observations are consistent with the presented results.

Finally, the influence of the number of load cycles on fracture and PICC parameters is addressed by an additional simulation that consisted in the application of 20 load cycles after a single release of nodes ($\text{d}a = l = 8.56\mu\text{m}$). The results (Figure 12) showed that the normalized $\Delta\text{CTOD}_\text{p}$ presents a high convergence with respect to the number of load cycles, with an average difference between the first and twentieth cycles lower than 4%. In contrast, the crack opening load displayed a huge dependence, concluding that 15 to 20 cycles are necessary to reach converged (cycle-independent) values, what demonstrates a high computational cost inherent to ΔK_eff-based approaches that require P_op/P_max in comparison to the proposed methodology.

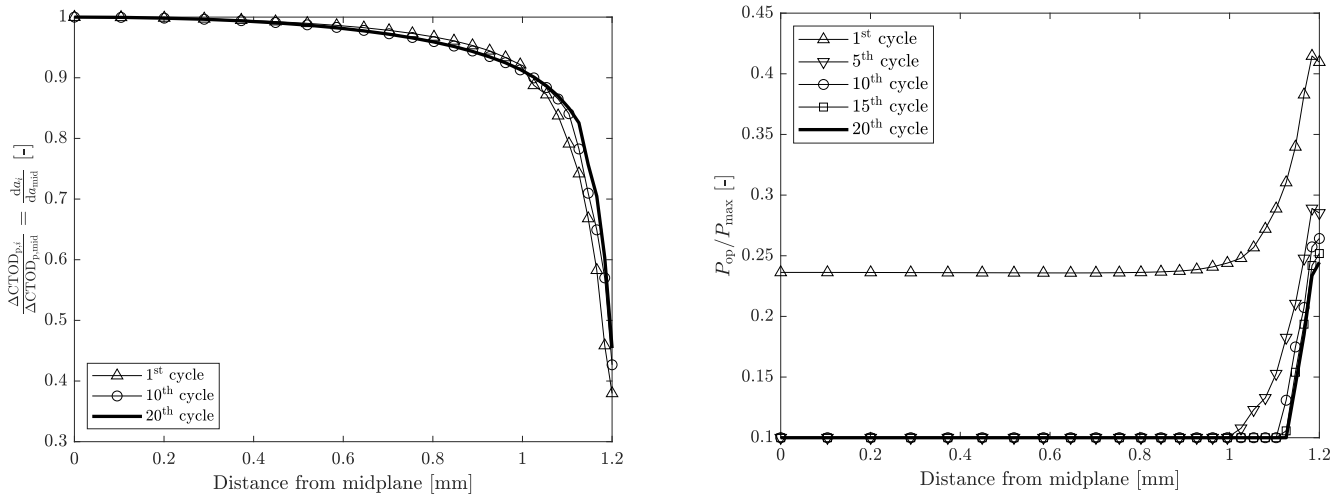

(a) $\Delta\text{CTOD}_{\text{p},i}/\Delta\text{CTOD}_{\text{p},j}$.

(b) $P_{\text{op}}/P_{\text{max}}$.

Figure 12: $\Delta\text{CTOD}_{\text{p},i}/\Delta\text{CTOD}_{\text{p},j}$ and $P_{\text{op}}/P_{\text{max}}$ after a single node release.

6. Conclusions

A methodology for the simulation of plasticity induced crack closure (PICC) and crack shape evolution (CSE) was proposed based on remeshing and mapping strategies for keeping the load history. The main novelty was the use of an elastic-plastic fracture parameter rather than the widely employed effective stress intensity factor range (ΔK_{eff}), what implies two relevant advantages: 1) a lower numerical effort, because a single finite element model needs to be developed and 2) a wider applicability, because large scale yielding scenarios can be analyzed. The methodology was illustrated through the application to an initially straight crack in a compact tension specimen subjected to small scale yielding, by using the plastic crack tip opening displacement range ($\Delta\text{CTOD}_{\text{p}}$) as the crack driving force for the first time in a 3D numerical study. It was concluded that:

- The proposed methodology is valid, based on the good numerical-experimental correlation of crack shapes (error of 2.65% in the tunneling distance) and the high agreement between the observed fracture and PICC parameter trends and the literature.
- $\Delta\text{CTOD}_{\text{p}}$ is an effective crack driving force, because it permits to predict crack shapes accurately, as mentioned in the previous point.
- $\Delta\text{CTOD}_{\text{p}}$ is an efficient crack driving force, because it shows faster convergence with applied load cycles than the crack opening load required by ΔK_{eff}. In fact, only one cycle had to be applied between node releases in order to determine the realistic crack shape evolution.

After the remeshing and mapping algorithms are optimized, the proposed methodology may help to understand better relevant phenomena related to crack propagation, such as the behavior of short cracks and the effect of stress ratio, mean stress and sample thickness.

Acknowledgement

Ikerlan's research has been supported by CDTI, depending by Ministerio de Ciencia e Innovación, through the "AYUDAS CERVERA PARA CENTROS TECNOLÓGICOS 2019" program, project MIRAGED with expedient number CER-20190001. This research center is certificated as CENTRO DE EXCELENCIA CERVERA. Furthermore, the work by R. Branco and F.V. Antunes has been sponsored by FEDER funds through the program COMPETE – Programa Operacional Factores de Competitividade – and by national funds through FCT – Fundação para a Ciência e a Tecnologia –, under the projects CENTRO-01-0145-FEDER-028789 and UIDB/00285/2020. Finally, the authors also want to acknowledge the financial support for short research stays provided by the University of Oviedo in cooperation with Banco Santander (2019).

References

[1] M. Luke, I. Varfolomeev, K. Lütkepohl, A. Esderts, Fatigue crack growth in railway axles: Assessment concept and validation tests, Engineering Fracture Mechanics 78 (5) (2011) 714 – 730, damage Tolerance of Railway Axles. doi:https://doi.org/10.1016/j.engfracmech.2010.11.024.
URL http://www.sciencedirect.com/science/article/pii/S0013794410004996

[2] H. Richard, M. Sander, B. Schramm, G. Kullmer, M. Wirxel, Fatigue crack growth in real structures, International Journal of Fatigue 50 (2013) 83–88. doi:10.1016/J.IJFATIGUE.2012.02.013.
URL https://www.sciencedirect.com/science/article/pii/S0142112312000746

[3] J. Šedek, R. Růžek, J. Raška, J. Běhal, Comparative Study of Prediction Methods for Fatigue Life Evaluation of an Integral Skin-Stringer Panel under Variable Amplitude Loading, Procedia Engineering 114 (2015) 124–131. doi:10.1016/J.PROENG.2015.08.050.
URL https://www.sciencedirect.com/science/article/pii/S1877705815016896

[4] X. Zhang, L. Li, X. Qi, J. Zheng, X. Zhang, B. Chen, J. Feng, S. Duan, Experimental and numerical investigation of fatigue crack growth in the cracked gear tooth, Fatigue & Fracture of Engineering Materials & Structures 40 (7) (2017) 1037–1047. doi:10.1111/ffe.12557.
URL http://doi.wiley.com/10.1111/ffe.12557

[5] T. L. Anderson, FRACTURE MECHANICS. Fundamentals and Applications, 3rd Edition, CRC-Taylor & Francis, Boca Raton, 2005.

[6] R. C. McClung, Finite element analysis of specimen geometry effects on fatigue crack closure, Fatigue & Fracture of Engineering Materials & Structures 17 (8) (1994) 861–872. arXiv:https://onlinelibrary.wiley.com/doi/pdf/10.1111/j.1460-2695.1994.tb00816.x, doi:10.1111/j.1460-2695.1994.tb00816.x.
URL https://onlinelibrary.wiley.com/doi/abs/10.1111/j.1460-2695.1994.tb00816.x

[7] J. Newman, A crack opening stress equation for fatigue crack growth, International Journal of Fracture 24 (4) (1984) R131–R135. doi:10.1007/BF00020751.

[8] G. Wang, A. Blom, A strip model for fatigue crack growth predictions under general load conditions, Engineering Fracture Mechanics 40 (3) (1991) 507–533. doi:10.1016/0013-7944(91)90148-T.
URL https://www.sciencedirect.com/science/article/pii/001379449190148T

[9] W. Guo, C. H. Wang, L. R. F. Rose, The influence of cross-sectional thickness on fatigue crack growth, Fatigue & Fracture of Engineering Materials & Structures 22 (5) (1999) 437–444. doi:10.1046/j.1460-2695.1999.00176.x.
URL https://onlinelibrary.wiley.com/doi/abs/10.1046/j.1460-2695.1999.00176.x

[10] W. Guo, C. H. Wang, L. R. F. Rose, The influence of cross-sectional thickness on fatigue crack growth, Fatigue & Fracture of Engineering Materials & Structures 22 (5) (1999) 437–444. doi:10.1046/j.1460-2695.1999.00176.x.
URL https://onlinelibrary.wiley.com/doi/abs/10.1046/j.1460-2695.1999.00176.x

[11] J. Newman, A finite-element analysis of fatigue crack closure, Tech. rep., National Aeronautics and Space Administration, Hampton (1974).

[12] R. McClung, H. Sehitoglu, On the finite element analysis of fatigue crack closure—2. numerical results, Engineering Fracture Mechanics 33 (2) (1989) 253 – 272. doi:https://doi.org/10.1016/0013-7944(89)90028-3.
URL http://www.sciencedirect.com/science/article/pii/0013794489900283

[13] R. Seifi, R. Hosseini, Experimental study of fatigue crack growth in raw and annealed pure copper with considering cyclic plastic effects, Theoretical and Applied Fracture Mechanics 94 (2018) 1–9. doi:10.1016/J.TAFMEC.2017.12.003.
URL https://www.sciencedirect.com/science/article/pii/S016784421730441X

[14] W. Mills, R. Hertzberg, The effect of sheet thickness on fatigue crack retardation in 2024-t3 aluminum alloy, Engineering Fracture Mechanics 7 (4) (1975) 705 – 711. doi:https://doi.org/10.1016/0013-7944(75)90026-0.
URL http://www.sciencedirect.com/science/article/pii/0013794475900260

[15] J. C. Newman Jr, C. A. Bigelow, K. N. Shivakumar, Three-dimensional elastic-plastic finite-element analyses of constraint variations in cracked bodies, Tech. rep., National Aeronautics and Space Administration, Hampton (1993).

[16] J. Costa, J. Ferreira, Effect of stress ratio and specimen thickness on fatigue crack growth of CK45 steel, Theoretical and Applied Fracture Mechanics 30 (1) (1998) 65–73. doi:10.1016/S0167-8442(98)00044-5.
URL https://www.sciencedirect.com/science/article/pii/S0167844298000445

[17] C. Gardin, S. Fiordalisi, C. Sarrazin-Baudoux, J. Petit, Numerical simulation of fatigue plasticity-induced crack closure for through cracks with curved fronts, Engineering Fracture Mechanics 160 (2016) 213 – 225. doi:https://doi.org/10.1016/j.engfracmech.2015.11.023.
URL http://www.sciencedirect.com/science/article/pii/S0013794416301643

[18] J. Skinner, S. Daniewicz, Simulation of plasticity-induced fatigue crack closure in part-through cracked geometries using finite element analysis, Engineering Fracture Mechanics 69 (1) (2002) 1 – 11. doi:https://doi.org/10.1016/S0013-7944(01)00115-1.
URL http://www.sciencedirect.com/science/article/pii/S0013794401001151

[19] S. Roychowdhury, R. H. Dodds, A numerical investigation of 3-d small-scale yielding fatigue crack growth, Engineering Fracture Mechanics 70 (17) (2003) 2363 – 2383. doi:https://doi.org/10.1016/S0013-7944(03)00003-1.
URL http://www.sciencedirect.com/science/article/pii/S0013794403000031

[20] A. Gonzalez-Herrera, J. Zapatero, Tri-dimensional numerical modelling of plasticity induced fatigue crack closure, Engineering Fracture Mechanics 75 (15) (2008) 4513 – 4528. doi:https://doi.org/10.1016/j.engfracmech.2008.04.024.
URL http://www.sciencedirect.com/science/article/pii/S001379440800115X

[21] K. Vor, C. Gardin, C. Sarrazin-Baudoux, J. Petit, Wake length and loading history effects on crack closure of through-thickness long and short cracks in 304l: Part ii – 3d numerical simulation, Engineering Fracture Mechanics 99 (2013) 306 – 323. doi:https://doi.org/10.1016/j.engfracmech.2013.01.014.
URL http://www.sciencedirect.com/science/article/pii/S0013794413000295

[22] D. Camas, J. Garcia-Manrique, A. Gonzalez-Herrera, Crack front curvature: Influence and effects on the crack tip fields in bi-dimensional specimens, International Journal of Fatigue 44 (2012) 41 – 50. doi:https://doi.org/10.1016/j.ijfatigue.2012.05.012.
URL http://www.sciencedirect.com/science/article/pii/S0142112312001958

[23] J. Garcia-Manrique, D. Camas, P. Lopez-Crespo, A. Gonzalez-Herrera, Stress intensity factor analysis of through thickness effects, International Journal of Fatigue 46 (2013) 58 – 66, characterisation of Crack Tip Stress Fields, Proceedings of the 1st Joint International Journal of Fatigue & Fracture of Engineering Materials & Structures conference, held in Forni di Sopra, UD, Italy, 7-9 March, 2011. doi:https://doi.org/10.1016/j.ijfatigue.2011.12.012.
URL http://www.sciencedirect.com/science/article/pii/S0142112311003379

[24] R. G. Chermahini, Three dimensional elastic-plastic finite element analysis of fatigue crack growth and closure, Ph.D. thesis, Old Dominion University (1986).

[25] T. J. Nykänen, Fatigue crack growth simulations based on free front shape development, Fatigue & Fracture of Engineering Materials & Structures 19 (1) (1996) 99–109. arXiv:https://onlinelibrary.wiley.com/doi/pdf/10.1111/j.1460-2695.1996.tb00935.x, doi:10.1111/j.1460-2695.1996.tb00935.x.
URL https://onlinelibrary.wiley.com/doi/abs/10.1111/j.1460-2695.1996.tb00935.x

[26] W.-Y. Lee, J.-J. Lee, Successive 3d fe analysis technique for characterization of fatigue crack growth behavior in composite-repaired aluminum plate, Composite Structures 66 (1) (2004) 513 – 520, twelfth International Conference on Composite Structures. doi:https://doi.org/10.

1016/j.compstruct.2004.04.074.
URL http://www.sciencedirect.com/science/article/pii/S0263822304001667

[27] R. Branco, F. Antunes, Finite element modelling and analysis of crack shape evolution in mode-i fatigue middle cracked tension specimens, Engineering Fracture Mechanics 75 (10) (2008) 3020 – 3037. doi:https://doi.org/10.1016/j.engfracmech.2007.12.012.
URL http://www.sciencedirect.com/science/article/pii/S0013794407004481

[28] R. Smith, J. Cooper, A finite element model for the shape development of irregular planar cracks, International Journal of Pressure Vessels and Piping 36 (4) (1989) 315 – 326. doi:https://doi.org/10.1016/0308-0161(89)90054-9.
URL http://www.sciencedirect.com/science/article/pii/0308016189900549

[29] X. Lin, R. Smith, Finite element modelling of fatigue crack growth of surface cracked plates: Part i: The numerical technique, Engineering Fracture Mechanics 63 (5) (1999) 503 – 522. doi:https://doi.org/10.1016/S0013-7944(99)00040-5.
URL http://www.sciencedirect.com/science/article/pii/S0013794499000405

[30] X. Lin, R. Smith, Finite element modelling of fatigue crack growth of surface cracked plates: Part ii: Crack shape change, Engineering Fracture Mechanics 63 (5) (1999) 523 – 540. doi:https://doi.org/10.1016/S0013-7944(99)00041-7.
URL http://www.sciencedirect.com/science/article/pii/S0013794499000417

[31] X. Lin, R. Smith, Finite element modelling of fatigue crack growth of surface cracked plates: Part iii: Stress intensity factor and fatigue crack growth life, Engineering Fracture Mechanics 63 (5) (1999) 541 – 556. doi:https://doi.org/10.1016/S0013-7944(99)00042-9.
URL http://www.sciencedirect.com/science/article/pii/S0013794499000429

[32] P. Paris, F. Erdogan, A critical analysis of crack propagation laws.

[33] R. BRANCO, D. M. RODRIGUES, F. V. ANTUNES, Influence of through-thickness crack shape on plasticity induced crack closure, Fatigue & Fracture of Engineering Materials & Structures 31 (2) (2008) 209–220. arXiv:https://onlinelibrary.wiley.com/doi/pdf/10.1111/j.1460-2695.2008.01216.x, doi:10.1111/j.1460-2695.2008.01216.x.
URL https://onlinelibrary.wiley.com/doi/abs/10.1111/j.1460-2695.2008.01216.x

[34] P. Yu, W. Guo, An equivalent thickness conception for prediction of surface fatigue crack growth life and shape evolution, Engineering Fracture Mechanics 93 (2012) 65 – 74. doi:https://doi.org/10.1016/j.engfracmech.2012.06.008.
URL http://www.sciencedirect.com/science/article/pii/S0013794412002627

[35] E. Wolf, Fatigue crack closure under cyclic tension, Engineering Fracture Mechanics 2 (1) (1970) 37 – 45. doi:https://doi.org/10.1016/0013-7944(70)90028-7.
URL http://www.sciencedirect.com/science/article/pii/0013794470900287

[36] P. Yu, W. Guo, An equivalent thickness conception for evaluation of corner and surface fatigue crack closure, Engineering Fracture Mechanics 99 (2013) 202 – 213. doi:https://doi.org/10.

1016/j.engfracmech.2012.12.013.
URL http://www.sciencedirect.com/science/article/pii/S0013794412004742

[37] M. Escalero, M. Muniz-Calvente, H. Zabala, I. Urresti, Suitability of constraint and closure models for predicting crack growth in generic configurations, Engineering Fracture Mechanics 225 (2020) 106808. doi:https://doi.org/10.1016/j.engfracmech.2019.106808.
URL http://www.sciencedirect.com/science/article/pii/S0013794419309762

[38] C.-Y. Hou, Simultaneous simulation of closure behavior and shape development of fatigue surface cracks, International Journal of Fatigue 30 (6) (2008) 1036 – 1046. doi:https://doi.org/10.1016/j.ijfatigue.2007.08.020.
URL http://www.sciencedirect.com/science/article/pii/S0142112307002514

[39] M.-H. Gozin, A.-K. Mehrdad, Quarter elliptical crack growth using three dimensional finite element method and crack closure technique, Journal of Mechanical Science and Technology 28 (2014) 2141–2151. doi:https://doi.org/10.1007/s12206-014-0503-x.
URL https://link.springer.com/article/10.1007/s12206-014-0503-x{#}citeas

[40] C. Gardin, S. Fiordalisi, C. Sarrazin-Baudoux, M. Gueguen, J. Petit, Numerical prediction of crack front shape during fatigue propagation considering plasticity-induced crack closure, International Journal of Fatigue 88 (2016) 68 – 77. doi:https://doi.org/10.1016/j.ijfatigue.2016.03.018.
URL http://www.sciencedirect.com/science/article/pii/S014211231630024X

[41] C.-Y. Hou, Development of a varying mesh scheme for finite element crack closure analysis, Engineering Fracture Mechanics 148 (2015) 42 – 59. doi:https://doi.org/10.1016/j.engfracmech.2015.09.009.
URL http://www.sciencedirect.com/science/article/pii/S001379441500507X

[42] P. Ljustell, Fatigue crack growth experiments on specimens subjected to monotonic large scale yielding, Engineering Fracture Mechanics 110 (2013) 138 – 165. doi:https://doi.org/10.1016/j.engfracmech.2013.07.006.
URL http://www.sciencedirect.com/science/article/pii/S0013794413002518

[43] C. Schweizer, M. Schlesinger, H. Oesterlin, V. Friedmann, P. Bednarz, C. Meilgen, J. Szwedowicz, Methodology for fatigue crack growth testing under large scale yielding conditions on corner-crack specimens, Engineering Fracture Mechanics 126 (2014) 126 – 140. doi:https://doi.org/10.1016/j.engfracmech.2014.04.032.
URL http://www.sciencedirect.com/science/article/pii/S001379441400143X

[44] U. Zerbst, M. Vormwald, R. Pippan, H.-P. Gänser, C. Sarrazin-Baudoux, M. Madia, About the fatigue crack propagation threshold of metals as a design criterion – a review, Engineering Fracture Mechanics 153 (2016) 190 – 243. doi:https://doi.org/10.1016/j.engfracmech.2015.12.002.
URL http://www.sciencedirect.com/science/article/pii/S0013794415006748

[45] D. T. Ngoula, M. Madia, H. Beier, M. Vormwald, U. Zerbst, Cyclic j-integral: Numerical and analytical investigations for surface cracks in weldments, Engineering Fracture Mechanics 198 (2018) 24 – 44, fracture mechanics-based determination of the fatigue strength of weldments. doi:https://doi.org/10.1016/j.engfracmech.2017.06.023.
URL http://www.sciencedirect.com/science/article/pii/S0013794417303582

[46] A. Papangelo, R. Guarino, N. Pugno, M. Ciavarella, On unified crack propagation laws, Engineering Fracture Mechanics 207 (December 2018) (2019) 269–276. doi:10.1016/j.engfracmech.2018.12.023.
URL https://doi.org/10.1016/j.engfracmech.2018.12.023

[47] F. V. Antunes, R. Branco, P. A. Prates, L. Borrego, Fatigue crack growth modelling based on ctod for the 7050-t6 alloy, Fatigue & Fracture of Engineering Materials & Structures 40 (8) (2017) 1309–1320. arXiv:https://onlinelibrary.wiley.com/doi/pdf/10.1111/ffe.12582, doi:10.1111/ffe.12582.
URL https://onlinelibrary.wiley.com/doi/abs/10.1111/ffe.12582

[48] J. Vasco-Olmo, F. Díaz, F. Antunes, M. James, Characterisation of fatigue crack growth using digital image correlation measurements of plastic ctod, Theoretical and Applied Fracture Mechanics 101 (2019) 332 – 341. doi:https://doi.org/10.1016/j.tafmec.2019.03.009.
URL http://www.sciencedirect.com/science/article/pii/S0167844218306554

[49] F. Antunes, S. Serrano, R. Branco, P. Prates, Fatigue crack growth in the 2050-t8 aluminium alloy, International Journal of Fatigue 115 (2018) 79 – 88, crack tip fields 4. doi:https://doi.org/10.1016/j.ijfatigue.2018.03.020.
URL http://www.sciencedirect.com/science/article/pii/S0142112318301129

[50] D. Camas, Numerical study of the three-dimensional behaviour of plasticity-induced crack closure phenomenon in bi-dimensional specimens, Ph.D. thesis, Universidad de Málaga (2013).

[51] D. Camas, J. Garcia-Manrique, B. Moreno, A. Gonzalez-Herrera, Numerical modelling of three-dimensional fatigue crack closure: Mesh refinement, International Journal of Fatigue 113 (2018) 193 – 203. doi:https://doi.org/10.1016/j.ijfatigue.2018.03.035.
URL http://www.sciencedirect.com/science/article/pii/S0142112318301270

[52] C.-Y. Hou, Plasticity-induced crack closure from surface to deep interior locations – a three-dimensional finite element study, Engineering Fracture Mechanics 195 (2018) 186 – 199. doi:https://doi.org/10.1016/j.engfracmech.2018.04.012.
URL http://www.sciencedirect.com/science/article/pii/S0013794417312663

[53] E. Giner, D. Fernández-Zúñiga, J. Fernández-Sáez, A. Fernández-Canteli, On the jx1-integral and the out-of-plane constraint in a 3d elastic cracked plate loaded in tension, International Journal of Solids and Structures 47 (7) (2010) 934 – 946. doi:https://doi.org/10.1016/j.ijsolstr.2009.12.012.
URL http://www.sciencedirect.com/science/article/pii/S0020768309004776

[54] C.-Y. Hou, Various remeshing arrangements for two-dimensional finite element crack closure analysis, Engineering Fracture Mechanics 170 (2017) 59 – 76. doi:https://doi.org/10.1016/j.engfracmech.2016.11.029.
URL http://www.sciencedirect.com/science/article/pii/S0013794416303666

[55] ASTM E647-15. Standard Test Method for Measurement of Fatigue Crack Growth Rates (2015).

[56] UNE-EN 10025-1:2006: Hot rolled products of structural steels - Part 1: General technical delivery conditions.

[57] ASTM E606. Standard practice for strain-controlled fatigue testing (2004).

[58] Standard Test Method for Measurement of Fracture Toughness.